Journal of
Engineering Sciences
Faculty of Engineering
Assiut University
JES
مجلة
العلوم الهندسية
كلية الهندسة
جامعة أسيوط
journal homepage: http://jesaun.journals.ekb.eg

Influence of Welding Conditions on Microscopic Structure, Microhardness in conjunction with Corrosion Resistance in solid-state joining process between Dissimilar Al Alloys AA5754 to AA5052

Received 8 October 2024; Revised 22 February 2025; Accepted 23 February 2025

Atef .E. Mahmoud[1]
H. T. Hussain[2]
I. M. Hassab-Allah[3]

Keywords
Dissimilar aluminum alloys
Corrosion resistance
Microstructure
Optimization
Taguchi

Abstract: 4.0 mm thick cold-rolled AA5754 and AA5052 aluminum alloy plates were joined together using Friction Stir Welding (FSW) under specific process conditions. Different Spindle speeds, welding speeds, and tilt angles. Tool pin profiles: cylindrical threaded, square, taper threaded, and triangular were utilized to create the joints. Their impact, on the internal structure, mechanical behavior, and resistance to corrosion were analyzed using optical microscopy (OM) and scanning electron microscopy (SEM), potentiodynamic polarization, and microhardness tests. The experiments are performed based on L16 orthogonal array considering the Taguchi technique for four design factors and four parametric levels. The welding parameters and tool pin profile play major roles in deciding the welding quality. This study reveals that the square pin profile tool creates welds that are both mechanically robust and free from metallurgical defects, outperforming other pin profiles. The square pin tool, when used with a rotational speed of 1000 rpm, delivers superior results, welding velocity of 56 mm/min, and tool tilt angle of 4^{o} gives high resistance to corrosion compared with other tool profiles.

1. Introduction

The automotive industry has recently shown a keen interest in the use of dissimilar aluminum alloys in the production of tailor welded blanks in order to minimize weight without increasing of the component costs [1]. The solid-state joining process utilizes a tool that does not get used up while rotating with the requisite head and probe size. The probe is inserted into plates to be joined as the tool rotates, the heat is generated by friction among the tool and plate's surfaces cause the weld plates to soften [2]. As the tool traverses the joint line, it mixes the softened material, leading to the creation of a solid-state weld without

[1] Assoc. professor, Dept. of Mining and Metallurgical Engineering. Eng., Assiut University, Assiut, Egypt. atef66@aun.edu.eg
[2] Mining & Metallurgical Engineering Department, Eng., Assiut University, Assiut, Egypt. Taghyan37@gmail.com
[3] Professor of Manufacturing Engineering, Mechanical Engineering Department, Eng., Assiut University, Assiut, Egypt. ibrahim.abdeldaiam@eng.aun.edu.eg

https://doi.org/10.21608/jesaun.2025.326883.1375

melting the material. The impact of friction stir welding (FSW) parameters on the microstructure, mechanical properties and corrosion resistance of aluminum alloys have been the subject of several investigations. In a study, Guido Di Bella et al. [3] examined how process parameters impact the properties of a friction stir welded (FSWed) joint between two disparate aluminum alloys, finding that square pins generate optimal material flow and stirring compared to triangular or stepped ones, but are susceptible to adhesion with stirred material, potentially causing defects.

Jamalian et al. [4] found that an unsound weld joint is created by very slight and very rising rotational speed (RPM) due to a lack of heat generation and a high level of turbulence, respectively. Another study was made by Khailiabad et al. [5] illustrated that the quality of FSWed joints improves with increasing the pin diameter. Zhang et al. [6] declared that the tensile strength of FSWed joints increases when the linear speed increases while the RPM decreases because of the grain size decreasing in the nugget zone. The effect of the tool tilt angle (TA) was analyzed by Krishna et.al. [7] And concluded that raising TA led to minimizing the joint defect. Gender [8] investigated the tool pin profile effect on the mechanical behavior, the result show that threaded cylindrical pin generates sound weld in comparison to a taper cylindrical pin profile. Naik et al. [9] determined that a hexagonal tool pin profile, combined with a RPM of 1363 rpm, a welding velocity of 715 mm/min, and a thrust load of 8 kN, resulted in enhanced resistance to corrosion and hardness. Aliha et al. [10] studied the influence of tool welding and RPM, along with the material type on the advancing and retreating sides of the weld, on the physical properties such as strength, hardness, and microstructure, concluding that placing the stronger material AA7277-T6 on the advancing side resulted in higher microhardness and tensile strength.

Kilic et al. [11] found that weld joint quality is significantly affected by process parameters, including tool design, RPM, welding speed (WT), and axial force. By optimizing these factors, weld strength can be boosted, and welding defects reduced. In research work by Çam et al. [12], two welding techniques, FSW and stands for Friction Stir Spot Welding (FSSW), were investigated. These methods offer considerable advantages over conventional fusion welding, such as the ability to weld various materials and achieve enhanced microstructural control. The use of FSW/FSSW is expected to become more widespread in the future to create hybrid structures with multiple alloys that were previously considered challenging or unfeasible to join.

Bella et al. [13] outlines a comprehensive and thorough overview of the primary process parameters and their impact on the final performance of a FSWed joint, considering both mechanical properties and microstructure. Hui [14] employed the Al-K2ZrF6 reaction system to fabricate in-situ Al3Zr/AA6082 particle-reinforced aluminum matrix composites using electromagnetic stirring melt reaction and FSW technology. The results revealed that the weld formation quality and tensile properties of the FSWed joints were optimal with welding parameters of 1400 rpm and 50 mm/min. Swetha and Padhy [15] investigated the influence of cylindrical, square, and tapered pin profiles on FSW of AA6061-T6

and AA2014-T4, while maintaining constant RPM and feed rate. Kumar et al. [16] investigated friction stir butt welds of AA6061 and AA7075 using a tapered pin, varying RPM, TA and axial force to determine the optimal weld settings.

Prakash and Das [17] optimized welding parameters using a Full Function Device (FFD), considering RPM, WT, displacement, and welding time. Impact strength (J) was the primary outcome, and statistical software ensured accurate and reliable joint quality evaluation. Mohapatra and Sarangi [18] conducted research that evaluated the effect of five RPM on the material characteristics of joints made with square, triangular, and cylindrical pin profiles in FSW. The results indicated that the square pin profile yielded the highest joint efficiency of 85%, which was superior to the triangular and cylindrical pin profiles.

Ramana and Sanke [19] studied the use of FSW to join high-strength AA2021 and AA7075 alloys with tools made of High-Speed Steel (HSS) and Tungsten Carbide (WC). They tested different welding parameters, including RPM (1120, 1400, and 1800 rpm) and feed rates (30, 40, and 50 mm/min). The results showed that welds made with HSS tools had better tensile properties, while WC tools caused tunnel defects in the welds. Kumar et al. [20] investigated friction stir butt welds of AA6061 and AA7075 aluminum alloys using a tapered pin. They studied the impact of RPM, TA, and axial force on weld quality. Experiments were conducted on 27 joints. They found that impact strength increased with RPM up to 900 rpm and then decreased and similarly increased with axial force up to 2.5 KN and then decreased. Increasing the TA also improved impact strength.

Alfattani et al. [21] studied the corrosion behavior of FSW joints between AA6061 and AA8011 aluminum alloys in salt spray and immersion environments. Mohammed et al. [22] studied the material characteristics and microstructure of an FSWed dissimilar aluminum alloy (AA2024-T3 to AA7075-0) through thickness produced by varying welding settings and three different FSW tool pin shapes. Their objective is to obtain the welds with the least amount of welding defects in the solid state by using the FSW, designing the tool pin profiles, and changing the RPM. This study by Rao et al. [23] focused on understanding the impact of heat generation during the FSW process of AA6061 and AA5052 aluminum alloys. Utilizing Deform-3D software, they simulated the FSW process across a range of RPM and feed rates. Through thermal analysis, they investigated the temperature distribution within the workpiece during the welding process, providing valuable insights into the heat generation and its potential effects on the final weld quality.

From the previous survey it can be noticed that few studies have been done on the non-heat treatable aluminum alloys 5xxx series. This aluminum alloys series are used frequently in marine applications and a lot of studies are still needed to obtain the FSW characteristics and the effects of welding process parameters on microstructure, microhardness and corrosion resistance of FSW joints obtained using aluminum alloys 5xxx series. Based on the latter research, it becomes obvious that a prediction method for maximizing the strength of FSWed joints by process parameters optimization is urgently needed. According to a literature review, the

relation between FSW process parameters and joint mechanical behavior represents an important key parameter that must be investigated and optimized. So, the aim of this research is to fabricate a dissimilar FSWed joint of AA5052 and AA5754 aluminum alloys, then optimizing the process parameters by Taguchi approach. The percentage contribution of a singular process parameter was evaluated using the ANOVA method.

2. Materials and methods

2.1. Experimental work

A joint of dissimilar aluminum alloys AA5052 and AA5754 was produced through FSW process by using the vertical milling machine. The power hacksaw machine was used to cut rolled plates of 4 mm thickness of AA5052 and AA5754 to the required size of (160 mm x100 mm) in this investigation. Welding was performed parallel to the base material's rolling direction. A single-pass welding technique was utilized to construct the joints. The material, received in an annealed state, was welded and tested without delay. The chemical compensation and mechanical properties of the used aluminum alloys are listed in Table (1) and Table (2), respectively.

Table 1: Chemical composition (in wt. %) of aluminum alloys

Materials	Mg	Si	Mn	Cr	Fe	Cu	Zn	Ti
AA5052	2.6	0.45	0.1	0.2	0.35	0.1	0.1	0.004
AA5754	3.17	0.61	0.03	0.37	0.26	1.53	0.2	0.15

Table 2: Mechanical properties of aluminum alloys

Alloy	**Ultimate tensile strength (MPa)**	**Yield strength (MPa)**	**Elongation (%)**	**Hardness (HV0.1)**
AA5052	190	79	22	47
AA5754	217	90	19	52

A typical non-consumable tool manufactured of H13 tool steel with a hardness of 55 HRC is used for FSW. In this study a tool pin with co-eccentric shoulder of four pin profiles; threaded cylindrical, threaded taper, square, and triangular were used. **Table (3) lists the tool specifications through the process of welding, AA5052 is positioned on** the **retreating side while AA5754 is located on the advancing side.**

Table 3: Tool specification and dimension

No	**Tool design**	Dimension
1	**Shoulder diameter**	20 mm
2	**Pin diameter**	6 mm
3	**Pin length**	3.8 mm
4	**Shoulder length**	40 mm

A light optical microscope (VERSAMET-3) was utilized to study the macro- and micro-structures of the materials in a FSWed joint. Specimens from the nugget zone (NZ), thermomechanically affected zone (TMAZ), heat affected zone (HAZ), and base metal (BM) of the welded joint were prepared by cutting and polishing with emery paper and a diamond compound. After preparation, the specimens were treated with Keller's reagent to expose their structural features. Microhardness tests were performed according to ASTM E384-17 on the cross section of joints along a direction perpendicular to the welding path.

To examine the corrosion behavior, all welded samples were immersed in a 3.5% sodium chloride (NaCl) solution. Polarization measurements were conducted on welded samples measuring 1 cm^2 in area and 3.5 mm wide. These samples were divided into three sections (WM, HAZ, and BM) using wire cutting. Each section was meticulously prepared for metallographic analysis through a series of grinding steps with progressively finer silicon carbide papers (100, 240, 360, 500, 600, 800, and 1000 grit), followed by polishing with alumina paste (0.3 µm) and diamond paste (1 µm). After rinsing with deionized water and drying with acetone, the samples underwent electrochemical testing.

Corrosion tests were performed at room temperature using a PGZ 100 potentiostat and a corrosion cell containing 500 ml of 3.5% NaCl solution, simulating seawater salinity. A platinum electrode served as the auxiliary electrode, while a calomel electrode (mercury and mercury chloride) acted as the reference electrode. The sample sections functioned as the working electrodes, and their steady-state open circuit potential (OCP) was recorded. Potentiodynamic scans were conducted from -1 mV to +1 mV versus OCP at a rate of 0.333 V/s, measuring corrosion currents. Corrosion current density (icorr) and corrosion potential (Ecorr) were determined from Tafel plots of potential versus the logarithm of corrosion current density (log I). The corrosion rate (CR) was calculated using Equation (1):

$$CR\ (mm/yr) = (0.00327 \times icorr \times eq.wt.)\ /D \qquad (1)$$

where icorr is the current density in $\mu A/cm^2$, D is the sample density in g/cm^3, and eq.wt. is the sample equivalent weight in grams.

2.1. Design of experiments

A Design of Experiments (DOE) approach, utilizing a Taguchi method and Minitab software, guides the FSW process. An L16 orthogonal array structure defines the DOE table. This study focuses on four key input factors: RPM, WT, tool TA, and pin profile. These factors and their limits are chosen based on preliminary experiments and a latter literature review and machine abilities which determine the parametric levels inside the minima-maxima range. Table (4) lists the welding parameters and their levels in detail. While Table (5) lists the FSW design parameters according to DOE used in the present experimental work.

Table 4: Control parameters for FSW process

Parameter	Units	Level			
		-2	-1	0	+1
RPM	rpm	710	1000	1400	2000
WT	mm/min	20	40	56	80
TA	degree	1º	2º	3º	4º
Pin profile	-	cylindrical threaded	square	tapered threaded	triangular

Table 5: FSW Design Parameters

Specimen No.	Pin profile	RPM (rpm)	WT (mm/min)	TA (º)
1	Cylindrical threaded	710	20	1
2		1000	40	2
3		1400	56	3
4		2000	80	4
5	Square	710	40	3
6		1000	56	4
7		1400	80	1
8		2000	20	2
9	Tapered threaded	710	56	1
10		1000	80	2
11		1400	20	3
12		2000	40	4
13	Triangular	710	80	3
14		1000	20	4
15		1400	40	1
16		2000	56	2

3. Experimental results and discussion

3.1. FSW process parameters Effect on the microstructure evolutions of welded joints

All the joints fabricated using square pin profiled tool are found to be free from defects irrespective of WT used (these results agree with experimental results obtained in ref. [8]). Figures 1 and 2 display both OM and SEM micrographs of the nugget zone (NZ) of FSWed joints subjected to different welding parameters. The figures illustrate that the reinforcement particles in NZ of the FSWed joints were refined under various welding conditions. At a WT of 20 mm/min with a TA of 4°, the refinement effect is most pronounced, as seen in Figure 2-d. In contrast, at a WT of 40 mm/min with a TA of 2°, the weld nugget zone shows noticeable defects, with the reinforcement particles from the base material aggregating primarily in a rectangular shape, along with a few short rod-like formations, see Figure (1-a). The huge granular with metallic shine represents the secondary phase, it appears clearly in both sides (advancing and retreating) of the specimen. From the above figures it can be noticed that FSW, with low WT and high tilting angle produced good stirring and resulted in uniformly distributed and fine second phase particles (fine precipitates) see Figures (1-d) and (2-d), while in case of FSW using cylindrical threaded with low tilting angle 2º coarse

precipitates were formed, see Figures (1-a) and (2-b). During FSW, the plasticized material was stirred by the stirring head.

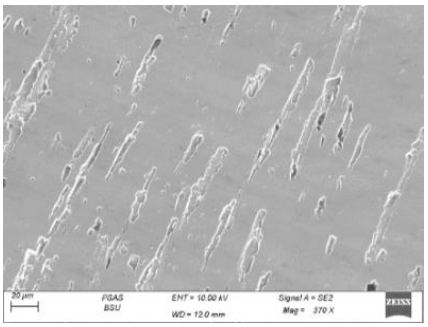

(a) WT = 40 mm/min, TA= 2º, and cylindrical threaded

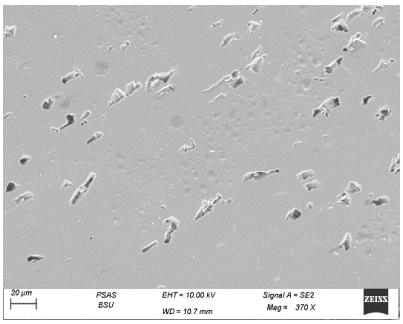

(b) WT = 56 mm/min, TA=4º, and square

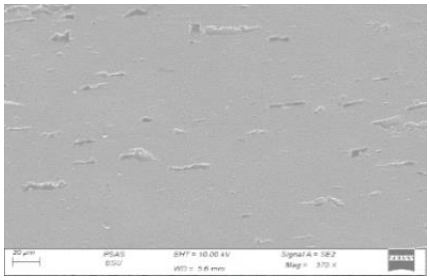

(c) WT= 80 mm/min, TA = 2º, and tapered threaded

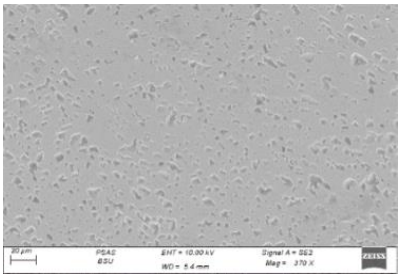

(d) WT =20 mm/min, TA = 4º, and triangular

Fig. 1: OM micrograph of nugget zone (NZ) for FSWed joints at RPM =1000 rpm for different pin profiles

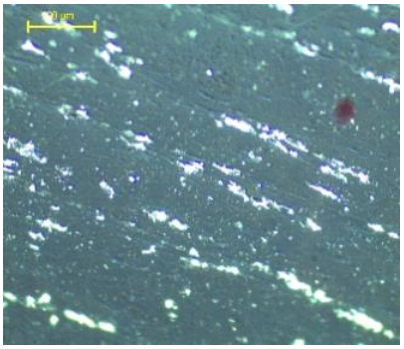

(a) WT = 40 mm/min, TA = 2º, and cylindrical threaded

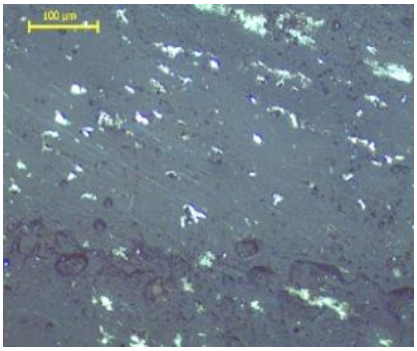

(b) WT= 56 mm/min, TA=4º, and square

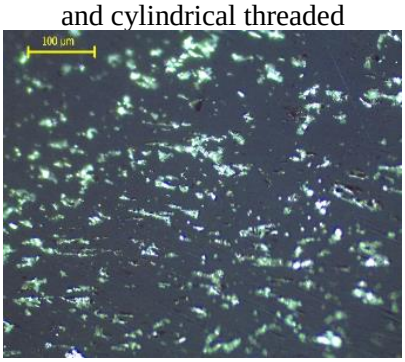

(c) WT= 80 mm/min, TA= 2º, and tapered threaded

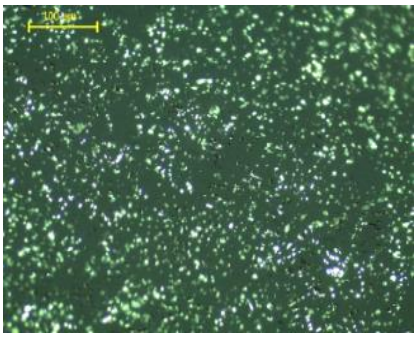

(d) WT=20 mm/min, TA = 4º, and triangular

Fig. 2: SEM micrograph of nugget zone (NZ) for FSWed joints at RPM =1000 rpm for different pin Profiles

3.2. Microhardness

Vickers microhardness profile is measured on the transverse section along a plane 0.5 mm under the shoulder plunge face of the two-butt edge joint sheets under an indenting load of 50-gf at loading time of 15 seconds. Figure 3 shows the maps of different cases of Vickers microhardness. According to Figure 3, the maps are plotted through two axes, the first axis in the horizontal line which illustrates the horizontal distance which is covered by the different zones of FSWed joints. On the other side, the second axis in the vertical line elucidates the vertical distance which is covered most zones of FSWed in the heights. As illustrated in Figure 3, microhardness maps for various pin profiles. Notably, the square pin profile (b) exhibits the lowest Vickers microhardness values compared to the other profiles (a), (c), and (d). This reduced hardness in the square profile may result from less effective material stirring and heat generation during the welding process, leading to a coarser microstructure that adversely affects hardness.

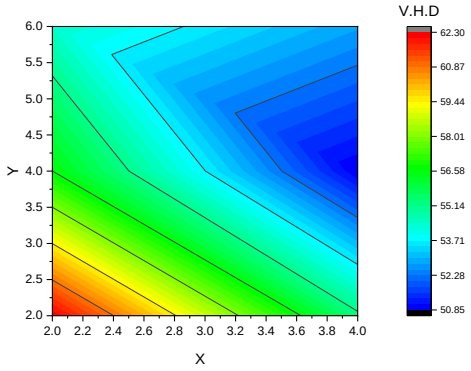

(a)WT= 40 mm/min, TA = 2º.

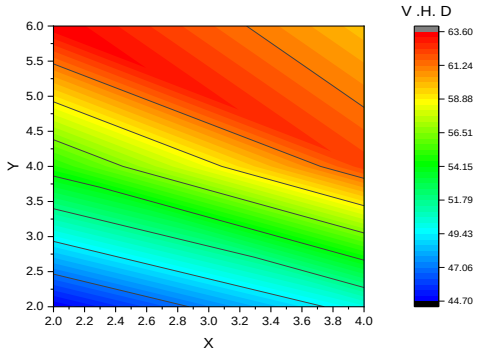

(b) WT = 56 mm/min, TA=4º.

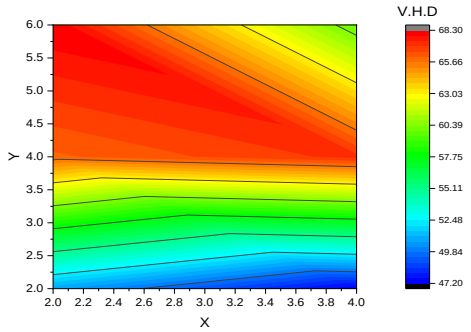

(c) WT = 80 mm/min, TA = 2º.

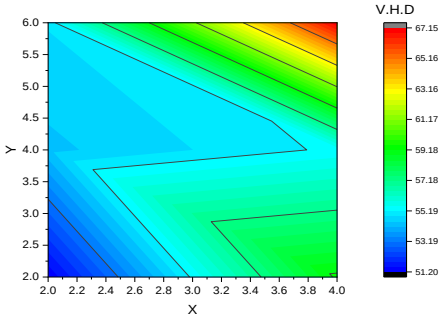

(d) WT =20 mm/min, TA = 4º.

Fig. 3: Microhardness maps of stirring zone (NZ) for FSW joints at RPM =1000 rpm for different pin profiles: (a) cylindrical threaded, (b) square, (c) tapered threaded, and (d) triangular.

The triangular pin profile consistently yields the highest maximum Vickers microhardness across all conditions, likely due to its enhanced stirring action and better material flow, resulting in finer grain structures and improved mechanical properties. Additionally, for the square pin profile, the combination of an RPM of 1000 rpm, a TA of 4°, and a WT 56 mm/min results in the minimum Vickers microhardness observed. This suggests that these specific parameters may not facilitate optimal stirring or heat input, leading to a detrimental impact on the hardness and overall performance of the weld.

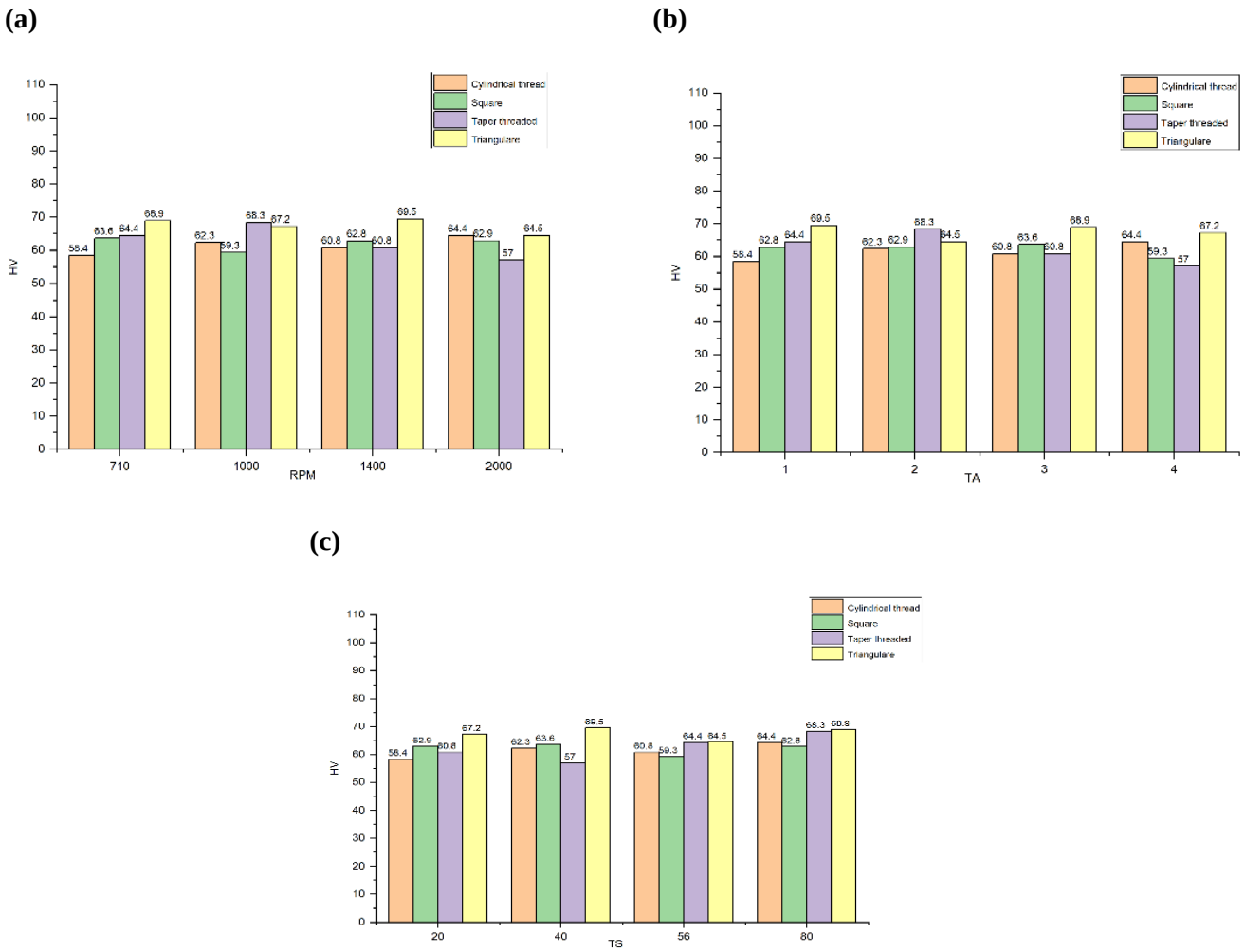

Fig. 4: The maximum Vickers microhardness values of nugget zone (NZ) for FSWed joints as a function of; (a) RPM (in rpm), (b) TA (in °), and (c) WT (in mm/min)

3.3 Corrosion tests

The potentiodynamic polarization corrosion test was conducted on FSWed joints, resulting in the Tafel curve displayed in Figure 5. The corrosion potential of each zone within the FSWed joint, from the Tafel curve data in Table 6, it is clear that a more negative corrosion potential signifies reduced corrosion resistance, crucial for assessing material durability. Localized corrosion typically begins as pitting and can progress into intergranular corrosion, both of which were evident in the test results.

Table 6: Corrosion rate, polarization resistance (Ohm), E corr (V), J corer (A/cm2), Bc (V/dec) and Ba (V/dec) of samples 2, 6, 10 and 14.

No.	Corr. rate (mm/year)	Polarization Resistance (Ohm)	E corr (V)	J corr (A/cm^2)	Bc (V/dec)	Ba (V/dec)
2	0.041	20090	-0.674	3.74E-6	0.172	0.067
6	0.028	29067	-0.779	2.62E-6	0.254	0.060
10	0.062	10864	-0.737	5.69E-6	0.118	0.060
14	0.041	20832	-0.792	3.79E-6	0.155	0.075

The accompanying scanning electron microscopy (SEM) images of the FSWed joints under various conditions and after the corrosion test are also displayed in Figure 6. The results

indicate that the lowest weight loss in NZ occurred with the square tool profile at RPM of 1000 rpm, a WT of 56 mm/min, and a TA of 4° (specimen no. 6). This reduced weight loss suggests that this configuration provided better corrosion resistance, likely due to the refined microstructure and uniform particle distribution achieved with these parameters. In contrast, the highest weight loss in NZ was observed with the tapered threaded pin profile (specimen no. 10), indicating that this configuration may have led to a coarser microstructure or less effective stirring, resulting in poorer corrosion resistance. Overall, these findings highlight the significant influence of tool RPM and tool profile on the corrosion behaviour of FSWed joints. Based on Figure 7, it is evident that pitting corrosion is present on the welded surfaces produced by the cylindrical threaded profile. This occurrence may be attributed to several factors, including the microstructural characteristics of the welds and the presence of coarse precipitates that can act as localized corrosion initiation sites. The cylindrical threaded profile design may have hindered optimal stirring and heat distribution in the FSW process, resulting in a non-uniform microstructure more susceptible to localized corrosion.

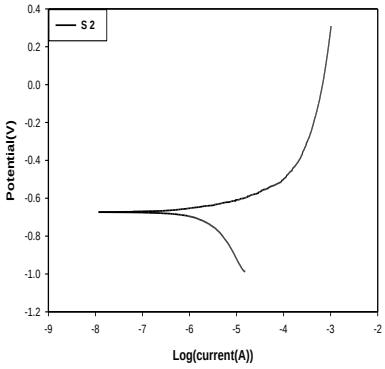

(a)WT= 40 mm/min, TA = 2º, and cylindrical threaded

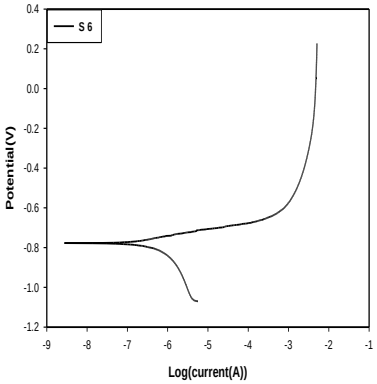

(b)WT = 56 mm/min, TA=4º, and square

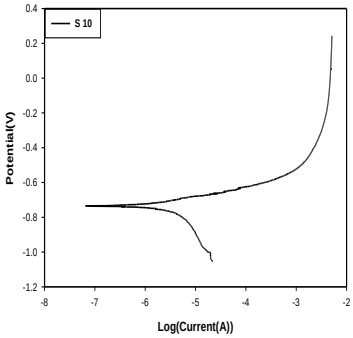

(c) WT= 80 mm/min, TA = 2º, and tapered threaded

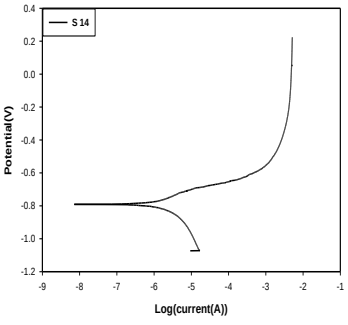

(d)WT =20 mm/min, TA = 4º, and triangular

Fig. 5: Potentiodynamic polarization curves of dissimilar FSWed joints at RPM =1000 rpm for different pin profiles.

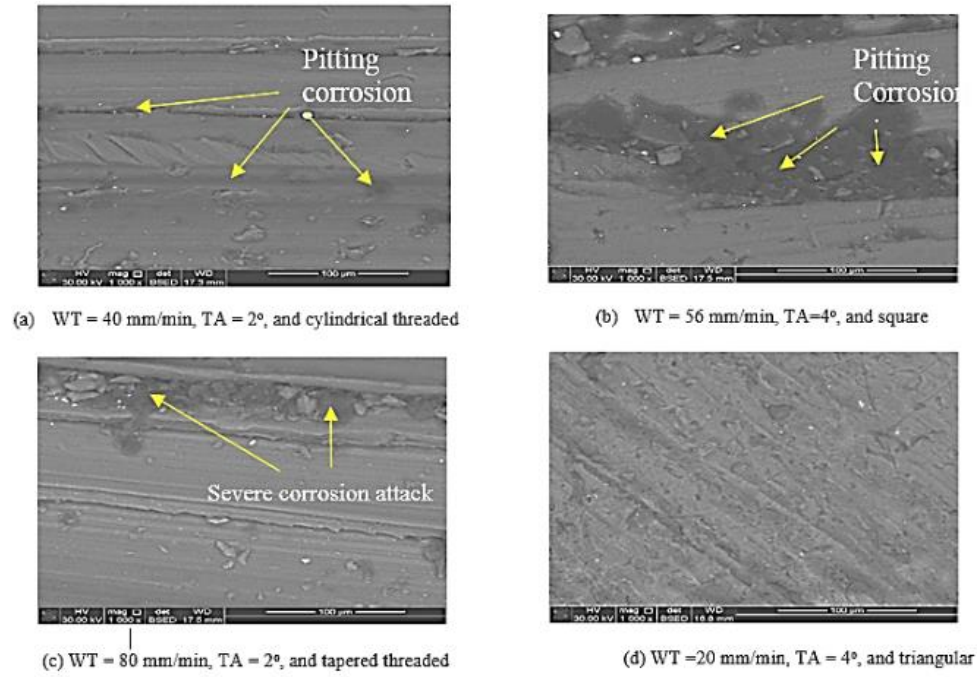

Fig. 6: SEM images of corroded

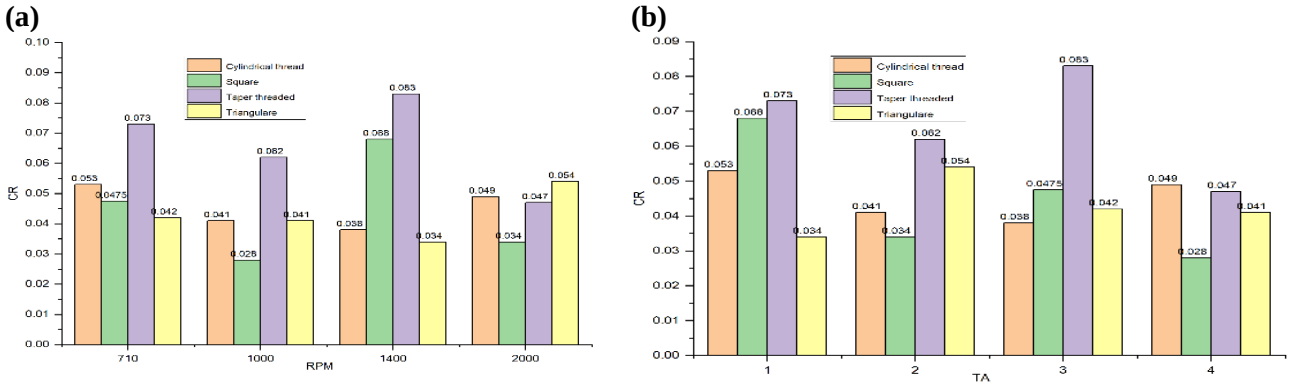

Fig. 7: The values of the corrosion rates for the four pin profiles used; (a) RPM (in rpm), and (b) TA (in °).

Conversely, minor pitting corrosion was noted on the welded surfaces produced using the square profile. Additionally, the electrochemical properties of the different regions in the welded joints can contribute to the variability in corrosion resistance, allowing pitting to initiate and propagate on these surfaces. Overall, the combination of these factors contributes to the observed pitting corrosion in the welded joints formed with these specific tool profiles. On the other hand, severe corrosion attacks were observed on the surfaces fabricated with the tapered threaded tool profile. This significant corrosion can be attributed to several factors, including the likely presence of a coarser microstructure and less effective material stirring during the welding process. The tapered threaded design may have resulted in uneven heat distribution and inadequate mixing of the base materials, leading to the formation of larger intermetallic precipitates that act as initiation sites for corrosion. Additionally, the electrochemical characteristics of the weld may have varied significantly across the surface, promoting localized corrosion. The combination of these factors

ultimately contributes to the pronounced corrosion attack observed in the joints produced with the tapered threaded tool profile, compromising their structural integrity. Simple pitting corrosion was observed on the welded surfaces produced by the triangular tool profile. This phenomenon can be attributed to the microstructural characteristics inherent to this tool design, which may not have provided the optimal stirring action needed to refine the grain structure effectively. Although the triangular profile enhances material flow, it may still allow for the presence of localized corrosion initiation sites due to variations in microstructure or the presence of precipitates. Additionally, the electrochemical potential differences between the matrix and the intermetallic phases can lead to localized attack, resulting in the observed pitting corrosion. Overall, while the triangular tool profile can offer advantages in terms of stirring, the specific conditions during welding may have still led to susceptibility to simple pitting corrosion. Figure 7 illustrates the correlation between the corrosion rate (CR) at tool profiles with varying TA and RPM. First, let's examine the relationship between the corrosion rate and the TA as increased from 1 to 4, the corrosion rate decreased due to several factors: a higher TA can reduce the contact area between the tool and the material, leading to less friction and wear; it may also enhance the drainage of corrosive agents from the surface; additionally, the change in angle can improve the distribution of protective coatings or materials, further mitigating corrosion. The minimum corrosion rate of 0.028 for the square tool profile at a 4° TA can be attributed to several factors: the square shape provides a more stable contact area, reducing wear and friction; the TA facilitates better drainage of corrosive substances, minimizing their contact with the tool surface; and this configuration likely promotes a more uniform distribution of protective films or coatings, further enhancing corrosion resistance. Second, let's examine the relationship between the corrosion rate and the RPM. The lowest corrosion rate observed at 1000 rpm with the square tool profile can be explained by several factors: the square design may optimize the tool's contact with the material, leading to reduced friction and wear; operating at 1000 rpm likely enhances the cooling effect, minimizing heat generation and corrosion; and this speed may also promote better lubrication, further protecting the tool surface from corrosive agents, thereby contributing to a lower corrosion rate.

4. Study limitations and suggestions for future work

This study is limited to relatively thick sheets 4.0 mm of aluminium alloys AA5052 and AA575. Only one tool shoulder diameter, one pin diameter, and four tool pin profiles; cylindrical threaded, square, taper threaded, and triangular were used. This study can be extended to different sheet thicknesses and different pin profiles, different pin and different shoulder diameters. Also, investigate how post-heat treatment enhances the properties of FSWed joints.

5. Conclusions

This research examines how different factors in a process affect FSW on the microstructure, mechanical properties, and corrosion resistance of dissimilar maritime structures made from AA5754-O and AA5052-O. Given that maritime structures face harsh marine conditions that accelerate corrosion and compromise their integrity, different FSW parameters were examined, including rotation rates ranging from 710 to 2000 RPM with speeds of 20 to 80 mm/min, TA between 1° and 4° and various tool pin profiles (cylindrical threaded, square, taper threaded, and triangular). A combination of optical microscopy (OM), scanning electron microscopy (SEM), potentiodynamic polarization, and microhardness tests were employed to assess the quality of the welded joints. Additionally, Taguchi analysis and Analysis of Variance (ANOVA) were utilized to identify the optimal process parameters based on an L16 orthogonal array, which encompassed four design factors and four parametric levels. Based on the main results and observations obtained, major conclusions drawn from the study are:

1. The optimum combinations of FSW parameters lead to welded joint defects free with proper mechanical and corrosion properties.
2. SEM analysis revealed prevalent intergranular corrosion, deep pitting, localized dissolution, and numerous corrosion pits on the specimens.
3. The elevated presence of intermetallic particles within the weld, a byproduct of the welding process, intensified galvanic corrosion coupling, consequently diminishing the weld's corrosion resistance.
4. An increase in the distribution of intermetallic particles within the weld matrix amplifies galvanic corrosion couples.
5. Minimal precipitates within the stir zone of an FSWed joint promotes passivation and enhance corrosion resistance. Conversely, an abundance of coarse precipitates obstructs passivation, leading to diminished corrosion resistance. For welding AA5052/AA5754 aluminum alloys at WT of 56 mm/min and a RPM of 1000 rpm, a square tool profile with a TA of approximately 4 degrees is recommended to achieve defect-free welds and superior corrosion resistance.
6. Welds produced using a square pin tool profile consistently exhibited no defects regardless of the WT employed.
7. Micrographs illustrate the corrosion damage observed after immersing FSW dissimilar aluminum joints (AA5052-O/AA5754-O) in 70 wt. % HNO_3 for 24 hours.

References

[1] R. K. Kesharwani, S. K. Panda, and S. K. Pal, "Experimental Investigations on Formability of Aluminum Tailor Friction Stir Welded Blanks in Deep Drawing Process", JMEPEG (2015) 24:1038–1049, ASM International,

[2] R. S. Mishra, P. S. De, and N. Kumar, "*Friction Stir Welding and Processing*". Cham: Springer International Publishing, 2014.

[3] Guido Di Bella, Federica Favaloro and Chiara Borsellino, "Effect of Process Parameters on Friction Stir Welded Joints between Dissimilar Aluminum Alloys: A Review", Metals 2023, 13, 1176. https://doi.org/10.3390/met13071176.

[4] Mohammadzadeh Jamalian, M. Farahani, M. K. Besharati Givi, and M. Aghaei Vafaei, "Study on the effects of friction stir welding process parameters on the microstructure and mechanical properties of 5086-H34 aluminum welded joints" *Int. J. Adv. Manuf. Technol.*, vol. 83, no. 1–4, pp. 611–621, Mar. 2016,

[5] M. Masoumi Khalilabad, Y. Zedan, D. Texier, M. Jahazi, and P. Bocher, "Effect of tool geometry and welding speed on mechanical properties of dissimilar AA2198–AA2024 FSWed joint", *J. Manuf. Process.*, vol. 34, pp. 86–95, Aug. 2018, doi: 10.1016/j.jmapro.2018.05.030.

[7] F. Zhang, X. Su, Z. Chen, and Z. Nie, "Effect of welding parameters on microstructure and mechanical properties of friction stir welded joints of a super high strength Al–Zn–Mg–Cu aluminum alloy", *Mater. Des.* vol. 67, pp. 483–491, Feb. 2015, doi: 10.1016/j.matdes.2014.10.055.

[8] G. G. Krishna, P. R. Reddy, and M. M. Hussain, "Effect of Tool Tilt Angle on Aluminum 2014 Friction Stir Welds", Global Journal of Research in Engineering: J General Engineering Volume 14 Issue 7 Version 1.0 Year 2014.

[9] S. Ugender, "Influence of tool pin profile and rotational speed on the formation of friction stir welding zone in AZ31 magnesium alloy", *J. Magnes. Alloys*, vol. 6, no. 2, pp. 205–213, Jun. 2018, doi: 10.1016/j.jma.2018.05.001.

[10] D. Balaji Naik, C. H. Venkata Rao, K. Srinivasa Rao, G. Madhusudan Reddy, and G. Rambabu, "Optimization of Friction Stir Welding Parameters to Improve Corrosion Resistance and Hardness of AA2219 Aluminum Alloy Welds", *Mater. Today Proc.*, vol. 15, pp. 76–83, 2019, doi: 10.1016/j.matpr.2019.05.027.

[11] M. R. M. Aliha, M. Shahheidari, M. Bisadi, M. Akbari, and S. Hossain, "Mechanical and metallurgical properties of dissimilar AA6061-T6 and AA7277-T6 joint made by FSW technique", *Int. J. Adv. Manuf. Technol.*, vol. 86, no. 9–12, pp. 2551–2565, Oct. 2016, doi: 10.1007/s00170-016-8341-x.

[12] Suleyman Kilic, Fahrettin Ozturk, Mehmet Fatih Demirdogen, "A comprehensive literature review on friction stir welding: Process parameters, joint integrity, and mechanical properties" , Journal of Engineering Research, Available online 6 September 2023,https://doi.org/10.1016/j.jer.2023.09.005.

[13] Gürel Çam, Vahid Javaher, Akbar Heidarzadeh, **"**Advances in FSW and FSSW of dissimilar Al-alloy plates", January 2023, Journal of Adhesion Science and Technology, Volume 37, 2023.

[14] Guido Di Bella, Federica Favaloro and Chiara Borsellino, "Effect of Process Parameters on Friction Stir Welded Joints between Dissimilar Aluminum Alloys: A Review", Metals 2023, 13, 1176. https://doi.org/10.3390/met13071176.

[15] *H.B. Mohammed , I.M. Naemah, A.J.S. Jomah , A.A.A.G. Alrubaiy* ,"Influence of tool pin profile and welding parameters on microstructure and mechanical properties of dissimilar friction stir welded AA2024 to AA7075 alloys",_Archives of Materials Science and Engineering 2023; 124 (1): 14-24, doi**:** 10.5604/01.3001.0054.3228

[16] Li Hui, Sun Caizhi, Wang Feng, Qiao Yuanpeng, Li Chuying, Xu Pinyi, Andrii Zatulovskiy, Volodymyr Shcheretskyi, "Study on Microstructure and Mechanical Properties of Friction Stir Welding Joints of In-Situ Al3Zr/AA6082 Particle-Reinforced Aluminum Matrix Composites", Arch. Metall. Mater. 68 (2023), 3, 907-919.

[17] S. Swetha, Chinmaya Padhy ,"Tool pin profiles effect on mechanical properties of friction stir welding of dissimilar aluminium alloys", Materialstoday,Volume 92, Part 2, 2023, Pages 1092-1098, https://doi.org/10.1016/j.matpr.2023.05.132.

[18] G. S. V. Seshu Kumar, Anshuman Kumar, S. Rajesh, Rama Bhadri Raju Chekuri, K. Ramakotaiah, "Optimization of FSW process parameters for welding dissimilar 6061 and 7075 Al alloys using Taguchi design approach", Int. J. Nonlinear Anal. Appl. 13 (2022) No. 1, 1011–1022.

[19] G. S. V. Seshu Kumar, Anshuman Kumar, S. Rajesh, Rama Bhadri Raju Chekuri, K. Ramakotaiah,

"Optimization of FSW process parameters for welding dissimilar 6061 and 7075 Al alloys using Taguchi design approach", Int. J. Nonlinear Anal. Appl. 13 (2022) No. 1, 1011–1022.

[20] Rami Alfattani , Mohammed Yunus , Ahmed Fathi Mohamed, Turki Alamro, Mohamed K Hassan , "Assessment of the Corrosion Behavior of Friction-Stir-Welded Dissimilar Aluminum Alloys" December 2021, Materials 15(1):26015(1):260.

[21] H.B.Mohammed , I.M.Naemah, A.J.S.Jomah , A.A.A.G. Alrubaiy ,"Influence of tool pin profile and welding parameters on microstructure and mechanical properties of dissimilar friction stir welded AA2024 to AA7075 alloys", Archives of Materials Science and Engineering 2023; 124 (1): 14-24,

[22] J.T. Chinna Rao, V. Harikiran, K.S.S. Gurudatta, M.V.D. Kumar Raju , "Temperature and strain distribution during friction stir welding of AA6061 and AA5052 aluminum alloy using deform 3D" Materials Today: Proceedings, Volume 59, Part 1, 2022, Pages 576-582.

[23] K. Elangovan and V. Balasubramanian, "Influences of tool pin profile and welding speed on the formation of friction stir processing zone in AA2219 aluminum alloy" journal of materials processing technology 200 (2008) 163–175.

[24] Di Bella, Guido, Federica Favaloro, and Chiara Borsellino. "Effect of process parameters on friction stir welded joints between dissimilar aluminum alloys: a review." Metals 13.7 (2023): 1176.

[25] Khan, Yusra Saman, et al. "Effect of Traverse Speed Variation on Microstructural Properties and Corrosion Behavior of Friction Stir Welded WE43 Mg Alloy Joints." Materials 16.14 (2023): 4902.

[26] Ilman, M. Noer. "Microstructure and mechanical properties of friction stir spot welded AA5052-H112 aluminum alloy." *Heliyon* 7.2 (2021).

[27] ABIDI, HAIDER, SERGEY KONOVALOV, and XIZHANG CHEN. "The effects of in-process cooling during friction stir welding of 7475 aluminium alloy." *Sains Malaysiana* 50.9 (2021): 2743-2754.

[28] Zamrudi, Firdausi H., and Asep R. Setiawan. "Effect of friction stir welding parameters on corrosion behaviour of aluminium alloys: an overview." *Corrosion Engineering, Science and Technology* 57.7 (2022): 696-707.